Image Reconstruction Algorithm using UT-ERT Dual Modality for Imaging Liquid and Gas

Fazlul Rahman Mohd Yunus[1,2], Ruzairi Abdul Rahim[1*], Anita Ahmad[1], Farah Aina Jamal Mohamad[1], Norhaliza Abdul Wahab[1], Leow Pei Ling[1], Mohd Hafiz Fazalul Rahiman[3], Chan Kok San[4], Jaysuman Pusppanathan[1], Nasarudin Ahmad[1], Nur Arina Hazwani Samsun Zaini[1], and Navintiran Rajan[1]

[1*] School of Electrical Engineering, Faculty of Engineering, Universiti Teknologi Malaysia, 81310 UTM Skudai, Johor, Malaysia.
[2] Advance Technology Training Center (ADTEC), Bandar Vendor Taboh Naning, 78000 Alor Gajah, Melaka, Malaysia.
[3] Faculty of Electrical Engineering Technology, Universiti Malaysia Perlis, Pauh Putra Campus, 02600 Arau, Perlis, Malaysia.
[4] Aimflex Berhad, Taman Teknologi Johor, 81400 Senai, Johor, Malaysia.

Corresponding author* email: ruzairi@utm.my
Available online 20 June 2022

ABSTRACT

Image reconstruction is one of significant element in the monitoring of a two-phase flow system. This paper presented image reconstruction algorithms for use in dual modality tomography (DMT) by combining ultrasonic tomography and electrical resistance tomography to visualise cross-sectional images of two-phase liquid/gas. The forward and inverse problems in image reconstruction are discussed, as well as various algorithms including linear back projection (LBP), filtered back projection (FBP), circular detection (CD), threshold (TH) and discrete wavelet transform (DWT) algorithms. Furthermore, the methods to assess the quality improvement of reconstructed image are also presented.

Keywords: Electrical resistance tomography, image reconstruction, ultrasonic tomography

1. Introduction

The development of dual-modality tomography system has gained a lot of attention among researchers in process industry. Rather than current single modality system, dual-modality tomography system has demonstrated its ability to distinguish between process components within an object space by utilising the same measuring technique. Ultrasonic tomography (UT) and electrical resistance tomography (ERT) have been popularly applied in numerous industrial processes, especially in multi-phase flow measurement and process monitoring [1]. Despite the fact that both approaches have demonstrated their utility in the process industry, a large number of researchers and institutions still invested their interest and time in the development of UT and ERT [2], [3]. Dual-modality tomography has been identified as a potential solution to the shortcomings of both UT and ERT methods by combining their greatest features. The construction of a system by applying these advantages is expected to satisfy the requirements for imaging multi-phase media.

Measurement data obtained from a set of several projection data of electrical resistance and ultrasonic transmission acquired from different angles around the pipe peripheral require mathematical process aiming to reconstruct the tomogram image [4]. The process was implemented due to its high computation speed and low computation cost [5]. In dual modality system, the acquired data obtained have to be properly interpreted as tomogram image. A forward problem is used to determine the theoretical voltage received by the sensors, whereas, the inverse problem is implemented to estimate the distribution of image from the sensor measurements. The following sections explain the forward problem and inverse problem, as well as the algorithm used. Finally, a new technique circular detection (CD) is introduced to improve the reconstruction image and fusion technique using discrete wavelet transform (DWT).

2. The Forward Problem

The purpose of the forward problem is to compute the theoretical output from sensed data and sensing area by discretizing an image plane into a grid of 64×64 pixels for each sensor projection. The theoretical output data from the sensor will then resemble the measurement area. The developed ERT-UT DMT system uses PVC sensor jig column with inner diameter that act as the region of interest (ROI) for measuring liquid/gas two-phase flow. The ROI area must first be converted into smaller elements known as pixels according to Equation 1,

$$P_x = \frac{D}{N} \tag{2}$$

where Px is the number of pixels, D is the diameter of inner pipe and N is the number of pixels in ROI. The square pixels will be used to display distribution of the normalized conductivity (ERT) and normalized voltage distribution (UTT) of each pixel to construct a tomogram image. Hence, the forward problem can be determined by modelling both UT and ERT sensor projections to their corresponding sensitivity map matrices [6].

2.1 Ultrasonic Projection

The ultrasonic tomography system utilized ultrasonic transceivers that can be functional as transmitters or receivers. As indicated in Figure 2.1, every transceiver is systematically arranged and distributed evenly around the circumference of the sensor jig. The ultrasonic transmitters will then send excitation pulses to the receiving pairs via sensor jig by using the transmission mode method. During each transmission, the transceivers transmit two cycles of pulse. In each transmitting transceiver controlled by a microcontroller, there will be corresponding receiving transceivers.

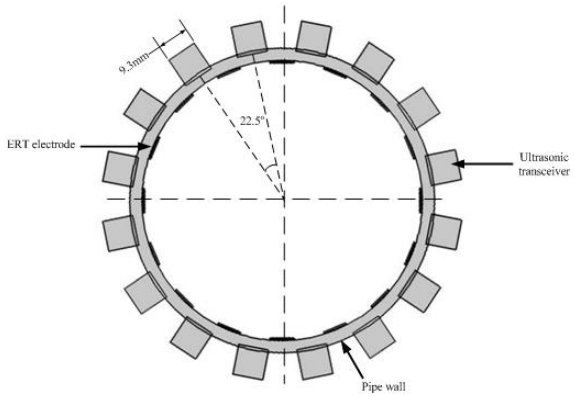

Figure. 1. Position of ultrasonic sensors

2.2 Ultrasonic Sensitivity Map

The ultrasonic transceiver forms sound waves that travelling through a medium with a particular beam divergence angle. The waves spread out in all directions across the medium before received by the receivers. Hence, sensitivity map is used to interpret the transmission and reception paths of active sensors within the projection area. Every pixel value in the sensitivity map represents the sensitivity area of the ultrasonic wave propagation, assuming that ultrasonic waves travel in straight lines with no obstructions in its travelling path.

2.3 ERT Sensitivity Map

The forward problem on ERT is being considered when determining the surface voltages resulting from a particular electrical conductivity distribution and current density on the excitation electrodes. To address the problem, it is a necessity to understand the mathematical model that defines the electric field inside the imaging area. The frequency of alternating current supplied into the sensing region is typically low to ignore the magnetic field effects and the material properties.

The sensitivity matrices in ERT represent the response of sensor to a single stimulus in sensing area. By employing different-conductivity material, the sensitivity map can be measured directly from the electrode and the response from each electrode pair is then collected [7]. The sensitivity maps can be obtained in a more practical and time-efficient method using Equation 2,

$$S_{i,j}(x,y)= \int_{P(x,y)} \frac{\nabla \emptyset_i}{A_i} \cdot \frac{\nabla \emptyset_j}{B_j} dxdy \quad (2)$$

where ϕ_i is the potential generated by the i electrodes driving the current and ϕ_j is the potential resulting from the j electrodes driving the current. Each electrode pair generates both currents, A_i and B_j.

3. Linear Back Projection Algorithm

Linear Back Projection (LBP) method is the most preferable by many researchers. Based on transposed matrix multiplication, it is the fastest and simplest algorithm to use because of its fast processing time compared to other algorithms. Although the LBP suffers from low quality reconstruction, this algorithm has proven due to its fast computation compared to more accurate iterative approaches [8]–[11]. Therefore, in imaging liquid/gas using dual modality technique, LBP could provide adequate imaging results for multiphase flow involving contrast or distinct materials such as water/gas.

Calibration process is initially executed before further process can be performed. Calibration occurs when the sensor jig column is filled with water (homogeneous medium) for both UT and ERT systems. The output matrices require standardisation, hence normalization has to be performed earlier. For each transmitting and receiving pair (UT), excitation and measurement pair (ERT), normalized sensitivity map is obtained using the following Equation 3 and Equation 4.

$$\bar{\boldsymbol{S}}_{\boldsymbol{T_x,R_x}} = \frac{S_{Tx,\ Rx}}{P_m} \quad (3)$$

$$\boldsymbol{VLBP}_{(x,y)} = \sum_{T_x=0}^{n} \sum_{R_x=0}^{n} \boldsymbol{V}_{\boldsymbol{T_xR_x}} \times \bar{\boldsymbol{S}}_{\boldsymbol{T_x,R_x}}(\boldsymbol{x,y}) \quad (4)$$

The $VLBP_{(x,y)}$ depicted the image concentration acquired from the LBP algorithm in 64×64 matrix, where n is equal to the sensitivity matrix dimension. The $\bar{S}_{T_x,R_x}(x,y)$ is the normalised sensitivity map for the projection of the transmitter T_x to the receiver R_x, and V_{T_x,R_x} is the value of sensor loss for the projection of transmitter T_x to receiver R_x. Sensor loss is the difference between the homogeneous flow and non-homogeneous flow. Homogenous flow refers to the full flow, whereas non-homogeneous flow is the flow condition that occurs when a phantom or object exists within the vertical sensor jig column. Equation 5 represents the V_{T_x,R_x} .

$$V_{T_x,R_x} = \frac{V_{cal}\,(T_x,R_x) - V_{meas}\,(T_x,R_x)}{V_{cal}\,(T_x,R_x)} \quad (5)$$

The $V_{cal}(T_x,R_x)$ is the electric potential measured in full water flow when T_x acts as an excitation electrode and R_x acts as receiver electrode, whereas $V_{meas}\ (T_x,\ R_x)$ is the electric potential measured in non-homogeneous flow when T_x acts as excitation electrode and R_x acts as the receiver electrode. The algorithm was then programmed with sensor loss value and sensitivity maps in order to produce image. In LBP, the sensor loss was then recorded by taking all independent measurements for a specific phantom. The tomogram image reconstruction is performed with LBP algorithm once all scans are completed.

Block diagram shown in Figure 2 illustrates a programming code for LBP algorithm to produce a tomogram image. The acquired measurement data from each modality were received in 2-D array and multiplied with a 64×64 normalised sensitivity map as in Equation 4. A while loop structure was implemented to perform loop execution for both UT and ERT. For each execution, the normalised sensitivity map is multiplied with the corresponding measurement data.

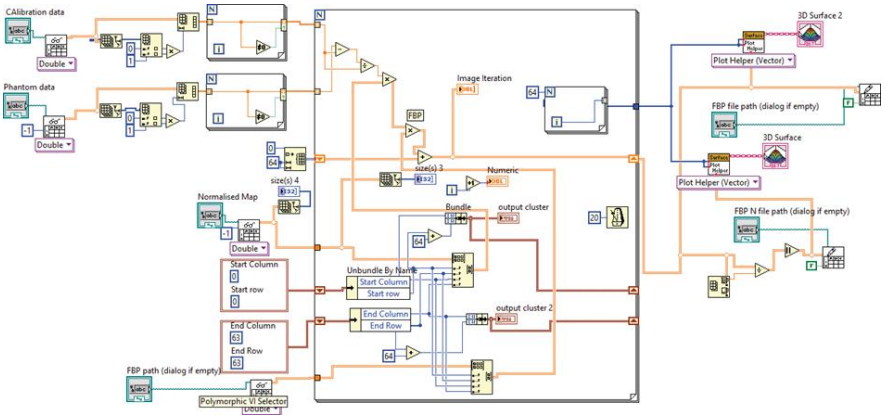

Figure. 2. Graphical code for LBP algorithm

4. Filtered Back Projection Algorithm

LBP has its limitations that it is unable to give a uniform concentration profile during a full flow or uniform distribution condition. This caused by the amount of the intensity received by the receivers are different due to the sensor's position and angle. Theoretically, in full flow condition or when the flow distribution is uniform, the concentration matrix should have constant value. However, LBP has resulted high concentration at the centre of the ROI. To overcome the problem, a filtered back projection (FBP) for full flow condition is implemented. A filter mask was introduced and has the same dimensions as the sensitivity matrices produced. The filter mask consists of weighting factor of the individual pixels to obtain a uniform concentration profile during full flow condition or when the sensor has equal outputs. The following equation is used to obtain the filter matrix.

$$\boldsymbol{F(x,y) = \frac{P_m}{VLBP_{(x,y)}} \quad ; VLBP_{(x,y)} > 0}$$

$$0 \quad ; VLBP_{(x,y)} = 0 \tag{6}$$

where:

$$VLBP_{(x,y)} = \sum_{T_x=0}^{n} \sum_{R_x=0}^{n} V_{T_xR_x} \times \bar{S}_{T_xR_x}(x,y)$$

Pm = Highest magnitude in pixel in matrix $VLBP_{(x,y)}$
$F(x,y)$ = Filter matrix

The Filtered Back-Projection algorithm is a product of the concentration profile obtained using the $VLBP_{(x,y)}$ and a filter matrix F (x, y) from Equation (6), represented as in Equation 7.

$$G_{FBP}(x,y) = F(x,y) \times VLBP(x,y) \tag{7}$$

5. Circular Detection Technique

Circles are common geometric structures of interest in modern computer vision applications. The use of Circle Hough Transform (CHT) is to locate circular patterns which represent gas column in liquid/gas two-phase 2-D tomogram images. Many circular algorithms have been investigated and developed by researchers. Nevertheless, the standard Hough Transform (HT) is the most desirable due to its robust techniques for circular detection. The technique can be extended to find multiple circles. In CHT technique, it takes information and a known radius and outputs the centre of the circle with the radius, which is the best fit information [12]. Then it is carried out by setting an accumulator grid, and all are initialized to zero. At this point, each data point votes on where the circle centre is possibly located. The circle can be written in Equation 8,

$$(x - a) + (y - b) = R^2 \quad (8)$$

where *a* is the centre of circle in the x-axis direction, *b* refers to the centre of circle in the y-axis direction and *R* are the variables. A surface in the *(a, b, R)* are three-dimensional parameter space which is created for each edge point *(x, y)* in the reconstructed image, where two of the three parameters refers to the position of the centre of detected circle *(a, b)* and the third one represents the circle of the radius R. The circle parametric is represented by Equation 9 and Equation 10.

$$x = a + r\cos(\theta) \quad (9)$$

$$y = b + \cos(\theta) \quad (10)$$

Therefore, the parametric space for the circle is denoted as R^3. The complexity of the HT rises as the number of parameters needed to define the image increase, as well as the dimensions involved. It is expected that CHT will produce triplets of (x, y, R) with high circles in the image. The edges must be determined first, and for every single edge point, a circle with the desired radius is obtained by assuming the edge point as the centre. Figure 3 shows a circle drawn in the parameter space.

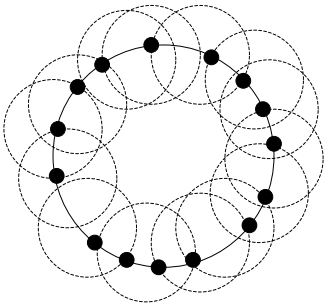

Figure. 3. Parametric space representation of a circle

The size of accumulator matrix is essentially the same as the parameter space at the perimeter coordinates, where 'a' value represents x-axis, 'b' value represents y-axis, and the radius of the drawn circle represents z-axis. During this process, every time a circle is drawn with the required radius around each edge point in the input image, the values in the accumulator will increase. When the process has completed all of the edge points and radiuses, it moves on to the accumulator. The accumulator numbers represent the number of circles derived from the coordinates of individual circles. This is illustrated in Figure 4.

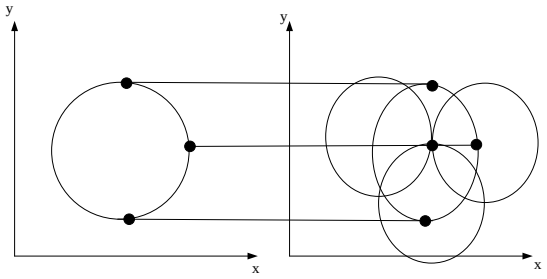

Figure. 4. Circular concepts in Hough Transform

6. Discrete Wavelet Transform

Image fusion algorithm aims to gather all information from different images of a captured scene from UT and ERT systems. Image fusion is defined as the process of combining two or more images into one while preserving the important characteristics of every single original images. In a variety of image processing operations such as object detection, feature extraction and segmentation, image fusion produces a new image that is more suitable for human and machine attention [13]. Image fusion techniques are classified into several types. It is determined by which domain is the fusion

is carried out, either in time domain or frequency domain. Each of these techniques can be classified into two types, spatial domain techniques and spectral domain techniques [14].

In producing image, fusion rule is a major criterion that must be carefully selected. Fusion rule is the critical component in image fusion, influencing the quality and speed of the fused image. In DMT, two reconstructed images obtained from UT and ERT can cause a little shape change since images were taken from different angles. The primary step during the fusion process is to register the input images to validate each pixel at correlated images has interconnection between images to resolve image drawback. These two images which have the same scene can register between them by connecting several control points. Then resampling is carried out by adjusting each image to same dimension and size before executing the fusion process [15]. Finally, an inverse transfer is performed if the image produced has been transferred to another domain. Figure 5 depicts the pre-processing of image fusion.

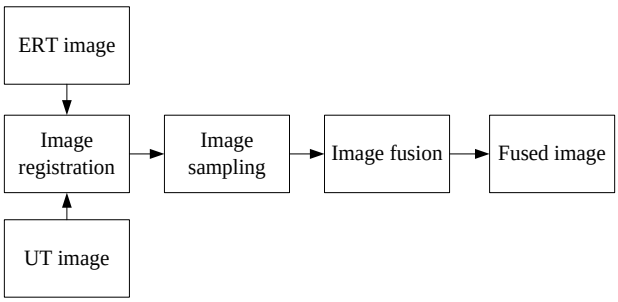

Figure. 5. Pre-processing of image fusion

Wavelet transform fusion is achieved by implementing the wavelet transforms W of the two registered input images $I_1(x, y)$ and $I_2(x, y)$ from UT and ERT with the determined fusion rule φ. The inverse wavelet transform W^{-1} is then computed, and the fused image $I(x, y)$ is reconstructed. This can be represented by Equation 11 and the process of image fusion is illustrated in Figure 6.

$$\boldsymbol{I(x,y) = W^{-1}[\varphi\{W(I_1(x,y)), W(I_2(x,y))\}]} \quad (11)$$

where I_1 is image 1, I_2 is image 2, W is discrete wavelet transform operator, and W^{-1} is inverse wavelet transform.

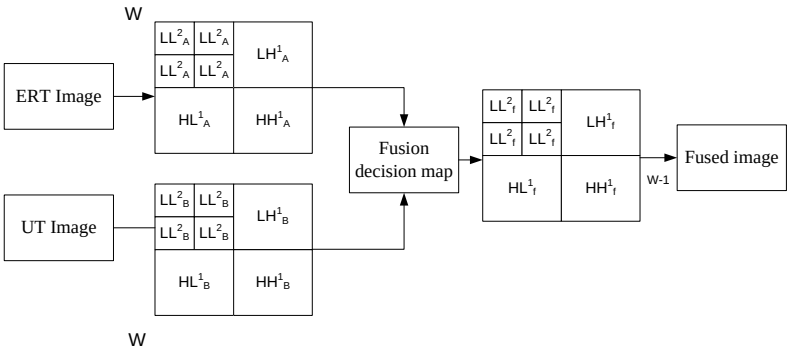

Figure. 6. Fusion two image using wavelet transform

Image fusion with wavelets aims to incorporate the decompositions of wavelet from the two original images (UT and ERT) by applying fusion methods to detail coefficients and approximation coefficients. The low frequency information is a significant component in the image because it provides the image with the most energy. In wavelet analysis, approximations are the low-frequency, high-scales components of the signal, whereas details are the high-frequency, low-scale components of the signal. Basic mathematical operations such as averaging, subtraction and addition are performed in image fusion techniques. The resultant image is obtained using the average rule by averaging each corresponding pixel in the input image from UT and ERT.

The graphical code programming for the wavelet fusion of DMT is illustrated in Figure 7. Image 1 and Image 2 represent reconstructed images from UT and ERT respectively. The 2-D image was computed to obtain multi-level integer wavelet transform of the image. The highest level of approximation coefficient was calculated together with detail

coefficient at all levels for the 2-D inputs. Then, the obtained coefficients were combined to compute the fusion image using inverse wavelet transform. The fusion rule implemented in the programming is shown in Table 1.

Table 1. Fusion rule setup for fusion image

Fusion Method	
Approximation	**Detail**
Mean	Max

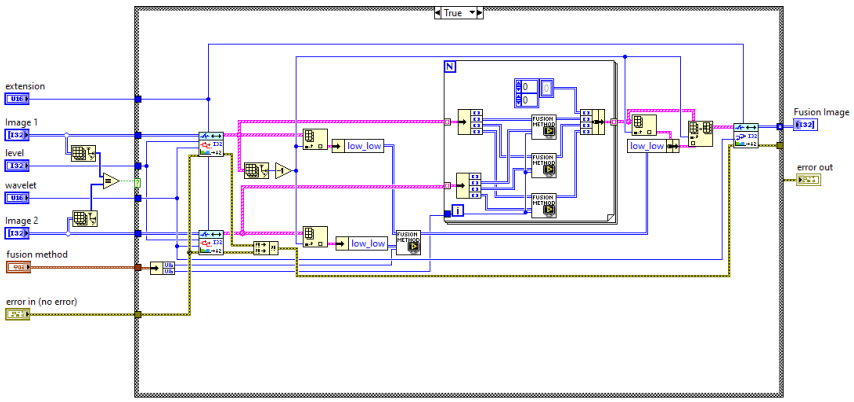

Figure. 7. Block diagram of image fusion using Wavelet transform

7. Image Quality Assessment

Image quality assessment is required as a significant tool to ensure the quality of the reconstructed tomogram images. Three most common methods in performing assessment images similarity-based technique are the mean squared error (MSE), cross-correlation (CC) and peak signal to noise ratio (PSNR). However, these techniques are quite ineffective to be recognized in visual quality as they use approach of estimated perceived errors [16]–[18] and are more suitable for single modality tomography system [19].

7.1 Mean Structural Similarity Index Method (MSSIM)

Mean Structural Similarity Index Method (MSSIM) is used to examine and evaluate reconstructed images from both UT and ERT on the single modality mode respectively. The MSSIM method compares similarity of two images from UT and ERT and produces output index ranging between zero and one (0-1). At higher index in MSSIM, it represents the reconstructed images closer compared to reference images [17], [20]. Equation 12 and Equation 13 show mathematical representation of MSSIM.

$$\boldsymbol{MSSIM}\ (\boldsymbol{X},\boldsymbol{Y}) = \frac{\mathbf{1}}{\boldsymbol{M}}\sum_{\boldsymbol{j=1}}^{\boldsymbol{M}} \boldsymbol{SSIM}(\boldsymbol{x_j},\boldsymbol{y_j}) \tag{12}$$

$$\boldsymbol{SSIM}(\boldsymbol{x},\boldsymbol{y}) = [\boldsymbol{l}(\boldsymbol{x},\boldsymbol{y})]^{\boldsymbol{\alpha}} \bullet [\boldsymbol{c}(\boldsymbol{x},\boldsymbol{y})]^{\boldsymbol{\beta}} \bullet [\boldsymbol{s}(\boldsymbol{x},\boldsymbol{y})]^{\boldsymbol{\gamma}} \tag{131}$$

where:
X = the reference image
Y = the distorted image
x and y = the image content at the jth local window
M = the image's number of local windows
$l(x,y)$ = the luminance comparison function
$c(x,y)$ = the contrast comparison function
$s(x,y)$ = the structural comparison function
α, β, γ = parameters for adjusting relative importance of the three components

7.2 Area Error

The area error (AE) is a common method for assessing the quality of reconstructed images in tomographic imaging systems. The fundamental idea of this method is similar as the image cross-sectional area for the reference model when compared to the reconstructed model. Furthermore, spatial image error in AE refers to the error of cross-sectional area or ROI of reference model compared to reconstructed images. If the reconstructed images are smaller compared to the reference image, thus, the result in AE will be a negative sign [21], [22]. Equation 14 shows the mathematical representation of the AE.

$$AE = \frac{N_a - N_m}{N_M} = \frac{\boldsymbol{N_a}}{\boldsymbol{N_m}} - \mathbf{1} \tag{14}$$

where *Na* represents the total number of effective pixels in the actual image and *Nm* represents the total number of effective pixels in reference image.

7.3 Thresholding Technique

Thresholding technique can be used in tomography applications to clarify the background from the target region [23]. Due to the non-linearity and ill-posed nature of the inverse problem, the quality of reconstructed image can be enhanced and the concentration areas of gas bubble can be identified by removing the noise pixels [24]. The thresholding technique requires the selection of a threshold ratio, which is the ratio of a pixel value to the maximum pixel value. Any pixel values outside the defined phase boundaries will be rounded down to zero (global thresholding approach). Equation 15 and Equation 16 describe the thresholding process for a particular reconstructed image.

$$\boldsymbol{Z_{Th}(x,y) = 0}, \qquad \boldsymbol{Z_{Th}(x,y) \leq \eta} \tag{15}$$

$$\boldsymbol{Z_{Th}(x,y) = Z_{Th}(x,y)}, \ \boldsymbol{Z_{Th}(x,y) \geq \eta} \tag{16}$$

8. Graphical User Interface (GUI) Development

Instead of applying text-based programming, LabVIEW is a graphical programming approach that enables users to visualize and obtain necessary information throughout various custom engineering user interfaces. The GUI that has been developed for the DMT is depicted in Figure 8. The visualization of projections from both excitation of UT and ERT, the sensitivity map distribution of both modalities, together with weight balance map, normalized sensitivity map, and fusion images can be observed from the developed GUI. The final reconstructed images for the two-phase liquid/gas are subsequently displayed with results of the quality assessment for each image.

In developing the GUI, the interface environment consists of interactive several pull-down menus, graphs and push buttons to ease selection and operation. Additionally, users can customize the interface to suit their requirements according to research environment.

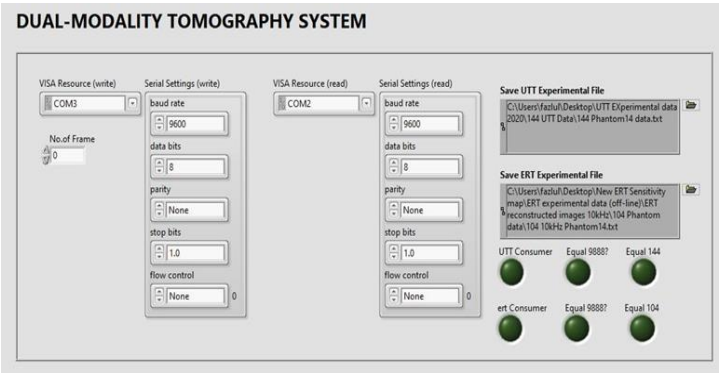

Figure. 8. Front panel of the DMT system using LabVIEW

9. Conclusions

This paper describes the image reconstruction techniques and algorithms for the UT-ERT dual modality by implementing the forward and inverse problems. From the forward problem, steps to generate the sensitivity map projection is explained. For the inverse problem, the process of reconstructing images using different algorithm such as LBP and FBP are discussed. The tomographic imaging obtained depicts the image of the examined area. A proposed technique for improving image circular detection and discrete wavelet transform for DMT image fusion has been elaborated. Further research is needed to implement the proposed technique and algorithm in various pipe shapes.

Acknowledgment

The authors would like to thank Universiti Teknologi Malaysia for supporting the research study and PROTOM research group for their assistance with this research paper.

References

[1] Dickin, F., & Wang, M. (1996). Electrical resistance tomography for process applications. *Measurement Science and Technology*, 7(3). doi: 10.1088/0957-0233/7/3/005.

[2] Wahab, Y. A., Ahmad, M. A., Rahim, R. A., & Rahiman, M. H. F. (2011). Application of transmission-mode ultrasonic tomography to identify multiphase flow regime. *International Conference on Electrical, Control and Computer Engineering*. doi: 10.1109/INECCE.2011.5953861.

[3] Rahim, R. A., Rahiman, M. H. F., & Taib, M. N. M. (2005). Non-invasive ultrasonic tomography: Liquid/gas flow visualization. *International Conference on Computers, Communications and Signal Processing with Special Track on Biomedical Engineering*, doi: 10.1109/CCSP.2005.4977199.

[4] Ai, M. (1996). Future of imaging technology. *Sensors Actuators, A: Physical*, 56(1–2). doi: 10.1016/0924-4247(96)01306-4.

[5] Rahiman, M. H. F., Rahim, R. A. & Tajjudin, M. (2006). Ultrasonic transmission-mode tomography imaging for liquid/gas two-phase flow. *IEEE Sensors Journal*, 6(6). doi: 10.1109/JSEN.2006.884549.

[6] Rahim, R. A., Nayan, N. M., & Rahiman, M. H. F. (2006). Ultrasonic Tomography System For Liquid/Gas Flow: Frame Rate Comparison Between Visual Basic And Visual C++ Programming. *Jurnal Teknologi*, 44(1). doi: 10.11113/jt.v44.380.

[7] Cao, Z., & Xu, L. (2012). Direct image reconstruction for 3D electrical resistance tomography by using the factorization method. *International Instrumentation and Measurement Technology Conference.* doi: 10.1109/I2MTC.2012.6229483.

[8] Steiner, G. (2006). Sequential Fusion of Ultrasound and Electrical Capacitance Tomography. *International Journal of Information and System Sciences*, 2(4).

[9] Asl, M. N., & Sadremomtaz, A. (2013). Analytical image reconstruction methods in emission tomography. *Journal of Biomedical Science and Engineering*, 6(1). doi: 10.4236/jbise.2013.61013.

[10] Wang, M. (2005). Impedance mapping of particulate multiphase flows. *Flow Measurement and Instrumentation*, 16(2–3). doi: 10.1016/j.flowmeasinst.2005.02.016.

[11] Shafquet, A., Ismail, I. & Karsiti, M. N. (2010). Study of bubble flow in an air-water two-phase flow by using Electrical Capacitance Tomography. *International Conference on Intelligent and Advanced Systems.* doi: 10.1109/ICIAS.2010.5716153.

[12] Zhou, B. (2016). Using vector quantization of hough transform for circle detection. *International Conference on Machine Learning and Applications.* doi: 10.1109/ICMLA.2015.94.

[13] Suraj, A. A., Francis, M., Kavya, T. S., & Nirmal, T. M. (2014). Discrete wavelet transform based image fusion and de-noising in FPGA. *Journal of Electrical Systems and Information Technology*, 1(1). doi: 10.1016/j.jesit.2014.03.006.

[14] Jinju, J., Santhi, N., Ramar, K., & Bama, B. S. (2019). Spatial frequency discrete wavelet transform image fusion technique for remote sensing applications. *Engineering Science and Technology International Journal*, 22(3). doi: 10.1016/j.jestch.2019.01.004.

[15] Tawade, L., Aboobacker, A. B., & Ghante, F. (2014). Image fusion based on wavelet transforms. *International Journal of Bio-Science and Bio-Technology*, 6(3). doi: 10.14257/ijbsbt.2014.6.3.18.

[16] Wang, Z., & Bovik, A. C. (2009). Mean squared error: Lot it or leave it? A new look at signal fidelity measures.

IEEE Signal Processing Magazine, 26(1). doi: 10.1109/MSP.2008.930649.

[17] Wang, Z., Bovik, A. C., Sheikh, H. R., & Simoncelli, E. P. (2004). Image quality assessment: From error visibility to structural similarity. *IEEE Transactions on Image Processing*, 13(4). doi: 10.1109/TIP.2003.819861.

[18] Horé, A. & Ziou, D. (2010). Image quality metrics: PSNR vs. SSIM. *International Conference on Pattern Recognition.* doi: 10.1109/ICPR.2010.579.

[19] Roshni, V. S. & Revathy, K. (2008). Using mutual information and cross correlation as metrics for registration of images. *Journal of Theoretical and Applied Information Technology*, 4.

[20] Wang, Z., Bovik, A. C., & Lu, L. (2002). Why is image quality assessment so difficult?. *IEEE International Conference on Acoustics, Speech and Signal Processing*, 4. doi: 10.1109/ICASSP.2002.5745362.

[21] Zulkarnay, Z., Rahiman, M. H. F., & Rahim, A. R. (2010). Simulation of the two-phase liquid–gas flow through ultrasonic transceivers application in ultrasonic tomography. *Sensors & Transducers Journal.*

[22] Huang, S. M. (1995). Error analysis of tomography systems a case study. *Process Tomography and Principals Techniques and Applications.*

[23] Kim, B. S., Khambampati, A. K., Kim, S., & Kim, K. Y. (2011). Image reconstruction with an adaptive threshold technique in electrical resistance tomography. *Measurement Science and Technology*, 22(10). doi: 10.1088/0957-0233/22/10/104009.

[24] Almazroui, S. & Wang, W. (2012). Microwave tomography for security applications. *International Conference on Information Technology and e-Services.* doi: 10.1109/ICITeS.2012.6216658.